



Experimental Challenges in Studying Hydrogen Absorption in Ultrasmall Metal Nanoparticles

Claudia Zlotea^{1*}, Yassine Oumellal¹, Karine Provost¹ and Camelia Matei Ghimbeu²

¹ CNRS, Institut de Chimie et des Matériaux Paris-Est (UMR7182), Université Paris Est, Thiais, France, ² CNRS, Institut de Science des Matériaux de Mulhouse (UMR7361), Université de Strasbourg, Université de Haute-Alsace, Mulhouse, France

OPEN ACCESS

Edited by:

Andrea Baldi,
Dutch Institute for Fundamental
Energy Research, Netherlands

Reviewed by:

Peter Ngene,
Utrecht University, Netherlands
Elsa Callini,
Comet ebeam Technologies,
Switzerland

*Correspondence:

Claudia Zlotea
claudia.zlotea@icmpe.cnrs.fr

Specialty section:

This article was submitted to
Hydrogen Storage and Production,
a section of the journal
Frontiers in Energy Research

Received: 20 April 2016

Accepted: 29 May 2016

Published: 27 June 2016

Citation:

Zlotea C, Oumellal Y, Provost K and
Ghimbeu CM (2016) Experimental
Challenges in Studying
Hydrogen Absorption in
Ultrasmall Metal Nanoparticles.
Front. Energy Res. 4:24.
doi: 10.3389/fenrg.2016.00024

Recent advances on synthesis, characterization, and hydrogen absorption properties of ultrasmall metal nanoparticles (defined here as objects with average size ≤ 3 nm) are briefly reviewed in the first part of this work. The experimental challenges encountered in performing accurate measurements of hydrogen absorption in Mg- and noble metal-based ultrasmall nanoparticles are addressed. The second part of this work reports original results obtained for ultrasmall bulk-immiscible Pd–Rh nanoparticles. Carbon-supported Pd–Rh nanoalloys in the whole binary chemical composition range have been successfully prepared by liquid impregnation method followed by reduction at 300°C. EXAFS investigations suggested that the local structure of these nanoalloys is partially segregated into Rh-rich core and Pd-rich surface coexisting within the same nanoparticles. Downsizing to ultrasmall dimensions completely suppresses the hydride formation in Pd-rich nanoalloys at ambient conditions, contrary to bulk and larger nanosized (5–6 nm) counterparts. The ultrasmall Pd₉₀Rh₁₀ nanoalloy can absorb hydrogen-forming solid solutions under these conditions, as suggested by *in situ* X-ray diffraction (XRD). Apart from this composition, common laboratory techniques, such as *in situ* XRD, DSC, and PCI, failed to clarify the hydrogen interaction mechanism: either adsorption on developed surfaces or both adsorption and absorption with formation of solid solutions. Concluding insights were brought by *in situ* EXAFS experiments at synchrotron: ultrasmall Pd₇₅Rh₂₅ and Pd₅₀Rh₅₀ nanoalloys absorb hydrogen-forming solid solutions at ambient conditions. Moreover, the hydrogen solubility in these solid solutions is higher with increasing Pd content, and this trend can be understood in terms of hydrogen preferential occupation in the Pd-rich regions, as suggested by *in situ* EXAFS. The Rh-rich nanoalloys (Pd₂₅Rh₇₅ and Pd₁₀Rh₉₀) only adsorb hydrogen on the developed surface of ultrasmall nanoparticles. In summary, *in situ* characterization techniques carried out at large-scale facilities are unique and powerful tools for in-depth investigation of hydrogen interaction with ultrasmall nanoparticles at local level.

Keywords: ultrasmall metal nanoparticles, hydride, solid solutions, hydrogen, X-ray absorption spectroscopy

INTRODUCTION

The control of materials at the nanoscale comprises a new frontier of opportunity in science and technology. The research interest in metallic nanoparticles lies in their many fascinating applications discovered in the recent years (Roduner, 2006). Promises and possibilities are wide ranging: nanocatalysts open new routes to various products, nanomagnets will store information for

modern computers, and nanoparticles will help drug delivery and medical imaging. However, the use of free nanoparticles raises the issue of their stability toward coalescence. From extensive research on the synthesis of nanoparticles, it became obvious that stabilized nanoparticles into light and porous supports/scaffolds are appropriate candidates to avoid/limit coalescence during utilization in the foreseen applications (de Jongh and Adelhelm, 2010; de Jongh et al., 2013; Zlotea and Latroche, 2013).

On another perspective, future energy landscape stringently requires the use of less-pollutant energy resources and the reduction of greenhouse emissions from fossil fuels. The emerging clean energy field comprises different renewable resources and hydrogen as one of the possible energy carriers (Eberle et al., 2009; Borgschulte, 2016). Three main challenges have been recently identified related to this field: analytical, materials, and system-related challenges (Borgschulte, 2016). The implementation of time- and space-resolved analytical methods with femto-second and nanometer resolutions, respectively, is opening new perspectives for in-depth characterization of functional materials. Similar to recent trends in materials science, this particular field is more and more reliant on novel nanomaterials due to their unique properties. Light and nanostructured materials (nanosized metals/alloys and hydrides along with nanoporous solids) are currently explored for their promising solid-state hydrogen storage and electrochemical conversion properties (Bérubé et al., 2007; de Jongh and Adelhelm, 2010; Cheng et al., 2012; Oumellal et al., 2014; Crivello et al., 2016; Sartori et al., 2016).

In this context, the insertion of hydrogen in metal nanoparticles is an important topic of fundamental research for both storage and sensing devices. However, the experimental study of hydrogen absorption in nanoparticles is very challenging, especially when dealing with ultrasmall nanoparticles. The latter ones are defined here as nanoparticles with average particle size ≤ 3 nm. The potential use of these metallic nanoparticles is largely unexplored in the hydrogen storage field, whereas the mainstream of studies on these materials is driven by heterogeneous catalysis. Both physicochemical properties of ultrasmall nanoparticles (structure, nanostructure, morphology, dispersion, etc.) and hydrogen absorption/desorption are difficult to characterize using classical laboratory techniques.

This report discusses the technical challenges in the synthesis and characterization of physicochemical properties of supported ultrasmall nanoparticles and their interaction with hydrogen gas (adsorption on surface, absorption in the volume with formation of solid solutions, and hydride phase). This is a fundamental study that focuses on the comprehension of hydrogen sorption mechanisms in ultrasmall nanoparticles. The first part will briefly review recent advances in the research on ultrasmall nanoparticles for hydrogen storage (both light- and noble metal-based nanoparticles). The second part will develop original results obtained on carbon-supported ultrasmall Pd–Rh nanoalloys (≤ 3 nm). Besides classical laboratory methods, fine characterization techniques based on large-scale facilities are requested for the *in situ* exploration of hydrogen insertion in these ultrasmall nanoparticles.

STATE OF THE ART: SYNTHESIS AND HYDROGEN ABSORPTION IN ULTRASMALL NANOPARTICLES

This first part will briefly review recent results reported for two types of ultrasmall nanoparticles: MgH_2 and noble metal-based supported clusters.

Synthesis

The synthesis of ultrasmall nanoparticles (≤ 3 nm) supported/embedded into porous hosts is very complex mainly due to coalescence issue and uncontrolled growth of nanoparticles. Among various methods for the synthesis of supported metal nanoparticles, the most widespread approach is the incipient wetness impregnation method: the porous support (typically carbon and metal organic framework) is impregnated with a solution of metal precursor, which is subsequently reduced using different reducing agents (H_2 , NaBH_4 , etc.) (Wilcoxon and Abrams, 2006; Roesler and Fischer, 2015). Another interesting technique is the melt infiltration of low temperature melting metals, such as Mg, into different porous carbon hosts (de Jongh and Eggenhuisen, 2013; Au et al., 2014). For both synthetic method many experimental parameters are playing a crucial role to ensure the stability toward coalescence and the high dispersion of such nanoparticles on the support: the porosity/surface chemistry of the support, the nature of metal precursor, the metal loading, and the synthesis conditions: temperature, reducing agent, etc. (de Jongh et al., 2007; Konarova et al., 2012; Zhao et al., 2012; Zlotea and Latroche, 2013).

For the preparation of supported MgH_2 nanoparticles by incipient wetness impregnation method, the porous host is impregnated with a commercial solution of MgBu_2 followed by hydrogenation under 50 bar H_2 pressure at 150°C (Nielsen et al., 2009; Zhang et al., 2009; Zlotea et al., 2011). Recently, we have clearly demonstrated that only the use of microporous carbon with high specific surface area (~ 2300 m^2/g) is favorable for the preparation of ultrasmall MgH_2 nanoparticles (≤ 3 nm) (Zlotea et al., 2015a). Moreover, the average nanoparticle size is strongly related to the metal amount and can be tuned from 1.3 to 3.0 nm for 15 and 25 wt% of Mg, respectively. The use of mesoporous carbon supports and/or high Mg loadings (>25 wt%) strongly increases the average size and broadens the particle size distribution (2–50 nm) (Oumellal et al., 2014). An important experimental difficulty is related to the air sensitivity of MgH_2 nanoparticle. All characterization measurements have to be performed under an inert atmosphere using air-tight sample holders.

The synthesis of ultrasmall noble metal-based nanoparticles supported on a porous host is well documented due to extensive study of such materials for catalysis and hydrogen sorption (Campesti et al., 2008; Narehood et al., 2009; Zlotea et al., 2010a; Contescu et al., 2011). Typically, a metal salt is used as precursor for porous host impregnation followed by a reduction step (H_2 , NaBH_4 , etc.) at different temperatures depending on the reducing agent (Narehood et al., 2009; Zlotea et al., 2010b, 2015b; Essinger-Hileman et al., 2011). For pure Pd and Rh nanoparticles, the use of high temperature, typically

above 300°C, as well as high metal loadings usually induces the growth of nanoparticles size and the increase of the particle size distribution (Zhao et al., 2012; Bastide et al., 2013; Zlotea et al., 2015b). Therefore, to prepare ultrasmall noble metal-based nanoparticles, low temperatures for the reduction step, moderate metal loadings, and highly porous supports are preferred.

Characterization of Physicochemical Properties

Besides the synthesis, the characterization of physicochemical properties of ultrasmall nanoparticles is also challenging. The most encountered difficulties are related to the observation of the crystalline structure by X-ray diffraction (XRD) together with the nanostructure, morphology, and dispersion on the porous support by transmission electron microscopy (TEM).

Light metal ultrasmall nanoparticles, such as MgH₂, have too short coherence lengths to diffract X-ray. The XRD patterns of the composites, containing MgH₂ nanoparticles with the average sizes of 1.3 and 3.0 nm, do not show any diffraction peaks from the expected MgH₂ tetragonal phase [see Figure 1 in Zlotea et al. (2015a)]. The patterns are very similar to the amorphous carbon diffractogram despite large Mg loading up to 25 wt%.

For noble metals, such as ultrasmall Pd and Rh nanoparticles, the XRD patterns clearly show the presence of broad diffraction peaks originating from the *fcc* structure (Zlotea et al., 2010b, 2015b). Contrary to light metal case, the photons are strongly scattered on the electron clouds of heavy elements and can diffract X-ray, despite their small size. The XRD measurements can be done either in air or under inert atmosphere to avoid surface oxidation during exposure to air.

Additionally, the classical TEM technique is very demanding for air sensitive nanoparticles that may also need cryogenic temperature measurements to avoid beam damage. For MgH₂ ultrasmall nanoparticles, the contrast with the carbon support is weak and therefore their size and dispersion can only be visible in dark-field TEM imaging. This is not the case for noble metal nanoparticles that can be noticed in bright-field TEM imaging.

Characterization of Hydrogen Absorption

The characterization of hydrogen absorption in ultrasmall nanoparticles is complex due to important size effects (Zlotea and Lacroche, 2013). The most commonly employed laboratory techniques to measure hydrogen sorption properties are isothermal kinetics, pressure–composition isotherms (PCI), differential scanning calorimetry (DSC), thermo-gravimetric analysis (TGA), and thermo-desorption spectroscopy (TDS). Several examples about size effect on the hydrogen absorption kinetics, thermodynamics, and capacity will be detailed below together with the most encountered difficulties at experimental level.

The kinetic modifications due to nanosizing are generally easy to notice by comparison to bulk counterpart if appropriate methodologies are used (TDS, TGA, isothermal kinetic curves, etc.) (Moretto et al., 2013). As a general trend, the nanosizing strongly improves the hydrogen absorption and desorption

kinetics of nanoparticles due to shorter diffusion paths of hydrogen within the nanoparticles and large surface area that increases the reaction rate of all surface-related phenomena (hydrogen dissociation and recombination) (Langhammer et al., 2010; Zlotea and Lacroche, 2013). For example, the onset temperature of hydrogen desorption for ultrasmall MgH₂ nanoparticles (~1.3 nm) occurs at a temperature about 245°C lower than the microcrystalline material (Zlotea et al., 2015a). Similar trend is also observed for Pd nanoparticles (~2.5 nm) that desorb hydrogen at around 50°C lower temperature than bulk material (Zlotea et al., 2010b).

As it concerns the changes in the thermodynamics, usually PCI and DSC measurements are employed for monitoring size effects. It is well known that phase transition in nanoscaled materials are no longer sharp, as usually observed for bulk (Roduner, 2006). Phase transitions are collective phenomena; therefore, they became less defined in small clusters. As a consequence, DSC measurements show almost vanishing peak transition with decreasing particle size to several nanometers. Indeed, the DSC peak corresponding to the hydrogen desorption from MgH₂ nanoparticles with ~3 nm became more shallow, as compared with bulk counterpart, and completely vanishes for ~1.3 nm MgH₂ clusters (Zlotea et al., 2015a). Nevertheless, the transition from hydride to metal phase (during hydrogen desorption) occurs at lower temperature compared with bulk with a strong size dependence, as expected for nanosized systems that may obey the *inverse size scaling law* (Roduner, 2006). From our previous reports on MgH₂, thermodynamic changes induced by nanosizing are difficult to assess due to important coalescence of nanoparticles observed during PCI measurements at high temperature (around 300°C) (Zlotea et al., 2013). This is due to significant mobility of light Mg atoms in Mg/MgH₂ nanoparticles at high temperature, whereas Mg possesses lower diffusivity when alloyed with heavier metal (Ni) in the nanoscaled phase Mg₂Ni. This may be understood in terms of weight of involved elements, since the diffusion rate is proportional to the inverse of squared mass of species.

When PCI curves can be measured without coalescence of nanoparticles (noble metal-based clusters), a typical example of size effect is the sloping of plateau in the PCI curves. It is well known that the plateau pressure (indicating the formation of a hydride phase) becomes steeper with decreasing the particle size of Pd (Sachs et al., 2001; Pundt and Kirchheim, 2006). Several explanations have been proposed, such as size-related changes in surface tension, interface stress due to stabilizers/scaffolds, or structural heterogeneities of the particles (Pundt and Kirchheim, 2006; Yamauchi et al., 2008). An important decrease of the enthalpy of hydride formation was earlier proposed for Pd nanoparticles with size around 2.6 nm (Yamauchi et al., 2008). Moreover, a narrowing of the two-phase regions of solid solution and hydride phases and a decrease in the critical temperature of the two-phase state have been reported for ultrasmall Pd nanoparticles (Yamauchi et al., 2008; Narehood et al., 2009). Nanosizing to ultrasmall dimensions even suppresses the hydride formation, as we recently proven for the supported nanoalloy Pd₉₀Co₁₀ ~2.4 nm, as compared with the bulk alloy counterpart

that forms a hydride phase at ambient pressure and temperature conditions (Zlotea et al., 2015c).

We recently reported a significant change in Rh–H thermodynamics induced by nanosize: Rh nanoparticles <2.3 nm can absorb hydrogen forming a hydride phase below 1 bar unlike bulk metal that needs 40 kbar hydrogen pressure to form a hydride phase at room temperature (Zlotea et al., 2015b). Rh nanoparticles with sizes ≥ 3 nm only form solid solutions with hydrogen under similar conditions.

Hydrogen absorption induced by nanosizing was also recently reported for another noble metal (Ir) that usually needs extremely high hydrogen pressure [several tens of kbar (Driessen et al., 1990)] to form a hydride phase. At nanoscale, ultrasmall Ir particles (~1.5 nm) can absorb large amount of hydrogen at ambient temperature and pressure (Kobayashi et al., 2012a; Zlotea et al., 2014). However, our experimental results point out to the formation of solid solutions with large hydrogen solubility (Zlotea et al., 2014) rather than a hydride phase, as previously claimed (Kobayashi et al., 2012a).

The size effect on the hydrogen storage capacity is not straightforward since it is strongly dependent on the induced thermodynamic changes. For noble metal nanoparticles, downsizing the metal particle size below 3 nm can be either beneficial or detrimental for the hydrogen sorption properties. The capacity of ultrasmall Rh and Ir nanoparticles noticeably increases, as compared with bulk at ambient pressure and temperature conditions due to thermodynamic changes, as discussed before. On the contrary, nanosizing Pd nanoparticles strongly decrease the hydrogen sorption capacity of the hydride phase from 0.7 to around 0.3 H/Pd and from bulk to 2 nm particles at ambient pressure and temperature conditions (Sachs et al., 2001; Pundt and Kirchheim, 2006; Yamauchi et al., 2008).

ULTRASMALL Pd–Rh NANOALLOYS

The second part will report original results obtained for carbon-supported ultrasmall Pd–Rh nanoalloys in the whole binary chemical composition range. The bulk Pd–Rh alloys have been already investigated for their interesting hydrogen storage performances as well as their promising catalytic properties as three-way converters in the exhaust pipes of gasoline-powered engines (Noh et al., 1991, 1993; Cappillino et al., 2014). However, very few studies have reported the effect of nanosizing on the hydrogen storage properties of these materials (Kobayashi et al., 2012b).

Materials and Methods

Synthesis

The synthesis of ultrasmall Pd–Rh nanoalloys is based on the incipient wetness impregnation method: a mesoporous carbon host was prepared by a soft template route, as described elsewhere (Zlotea et al., 2015c), followed by impregnation with an aqueous solution of a mixture of metal precursors ($\text{RhCl}_3 \cdot x\text{H}_2\text{O}$ and H_2PdCl_4) and subsequently reduced under Ar/H_2 flow at 300°C for 1 h. More details on the synthetic part of composites are given

in our previous study (Oumellal et al., 2016). Five compositions have been synthesized in the whole binary composition: $\text{Pd}_{90}\text{Rh}_{10}$, $\text{Pd}_{75}\text{Rh}_{25}$, $\text{Pd}_{50}\text{Rh}_{50}$, $\text{Pd}_{25}\text{Rh}_{75}$, and $\text{Pd}_{10}\text{Rh}_{90}$. The final metal composition is 10 wt% over the whole composite mass.

Hydrogen Sorption Measurements

Hydrogen sorption properties were determined by measuring the PCI at 20°C up to 1 bar of hydrogen pressure using an automated volumetric device (Autosorb IQ Quantachrome). Prior to any sorption measurement, the samples were treated under hydrogen atmosphere at 20°C to reduce the oxide layer at the surface of nanoparticles and subsequently degassed at 120°C to remove water molecules formed during this step (Ghimbeu et al., 2011). The hydrogen absorption/desorption is completely reversible for all samples. The hydrogen sorption capacity is expressed in wt% over the entire mass of sample.

X-Ray Diffraction

Structural characterizations were performed by XRD using a Bruker D8 Advance instrument (Cu- K_{α} , Bragg-Brentano geometry, Anton Paar chamber TTK450, and Văntec Position Sensitive Detector). *In situ* XRD measurements were performed under dynamic vacuum and 1 bar of hydrogen pressures at room temperature. The XRD patterns have been analyzed by the TOPAS software (Bruker AXS Topas 4.2) to determine the lattice parameters.

Transmission Electron Microscopy

The micro(nano)structural observations were performed by TEM with a 200-kV FEG TEM (FEI Tecnai F20 equipped with a Gatan energy Imaging Filter, resolution 0.24 nm). The nanoparticle size distribution and average size have been determined by statistical analyzes of several TEM images.

X-Ray Absorption Spectroscopy

The local structure of the Pd–Rh nanoalloys was investigated by X-ray absorption spectroscopy (XAS) in transmission mode on ROCK beam line at the SOLEIL synchrotron. The X-ray absorption spectra at the K edges of Pd and Rh were measured under H_2 and N_2 flow (30 ml/min) at room temperature with a typical edge jump between 0.4 and 0.8. Bulk Pd and Rh were also measured and used as references. The powder samples were placed inside the Lytle-type cell available on the beam line (Fontaine et al., 2013). The sample cell was connected to a gas distribution system that allows careful control of the gas mixture and the flow at atmospheric pressure. The samples were pretreated under hydrogen flow at room temperature to reduce the oxide layer at the surface of nanoparticles (Ghimbeu et al., 2011). The XAS data treatment and EXAFS refinements were performed by the help of the MAX program package ($E_0 = 24,350$ and $23,230$ eV for Pd and Rh K edges, respectively, Fourier transform range $4\text{--}14 \text{ \AA}^{-1}$) (Michalowicz et al., 2009, 2013). EXAFS fit was performed on first-sphere filtered spectra. Theoretical phases and amplitudes were computed with FEFF8 on the basis of Pd and Rh metal *fcc* structures (Ankudinov et al., 1998, 2003). Due to the close proximity of Rh and Pd in the periodic table and their similar atomic radius, it was not possible to distinguish Pd and Rh first neighbors

(NN), and we have used a unique (Pd/Rh)-NN shell. The refined parameters are the coordination number (N), the Debye–Waller factor (σ^2), and the distance between the absorbing atom (either Pd or Rh) and the first neighbors (R). The energy shift ΔE_0 was refined first for bulk Pd and Rh references (4.7 and 3.7 eV, respectively) and then fixed for further refinements. Statistical errors and error bars were evaluated as recommended by the IXS Standard and Criteria Subcommittee (Sayers, 2000). According to these recommendations, the goodness of fit was evaluated using the reduced $\Delta\chi^2$ minimum or quality factor (QF).

RESULTS

Crystalline Structure and Nanostructure

The XRD patterns of ultrasmall Pd–Rh nanoparticles are shown in **Figure 1**. Typical TEM images and histograms of particle size for all Pd–Rh nanoalloys are shown in Figure S1 in Supplementary Material. Although the diffraction peaks are very broad, XRD investigations prove that these nanoparticles adopt a *fcc* crystal structure ($Fm\bar{3}m$) typical for Pd–Rh bulk alloys (Raub, 1959). The *fcc* lattice parameter, as obtained from XRD, together with the average particle sizes, as determined by TEM, is listed in **Table 1**. The lattice parameters vary linearly with the composition, in agreement with bulk Pd–Rh alloys (Raub, 1959). This trend is typical for substitutional alloys and proves the formation of Pd–Rh nanoalloys in our synthetic conditions. To further confirm the formation of nanoalloys, EDX chemical analysis has been carried out for two samples: Pd₇₅Rh₂₅ and Pd₅₀Rh₅₀ (Figures S2 and S3 in Supplementary Material). From these analyzes, Pd and Rh are uniformly distributed on the carbon support and coexist within the same nanoparticles in both selected compositions. Quantitative EDX analysis for the Pd₅₀Rh₅₀ sample is very close to the nominal 50:50 with a dispersion of around 11 at%. These results confirm our claim of Pd–Rh nanoalloy formation. The TEM average particle sizes are between

1.5 and 3.0 nm thus, within our definition, these nanoalloys are ultrasmall nanoparticles.

Hydrogen Absorption

The hydrogen adsorption properties of Pd–Rh nanoalloys have been studied by volumetric method (PCI curves), *in situ* XRD and EXAFS. DSC analysis was unsuccessful for studying the hydrogen sorption in these nanomaterials due to issues discussed above (see Characterization of Hydrogen Absorption). The PCI curves measured up to 1 bar H₂ pressure and 20°C for all Pd–Rh composites and pristine carbon are plotted in **Figure 2**. For the sake of comparison, the PCI curve of pure Pd ultrasmall nanoparticles (average size ~2.5 nm) is also given. Interestingly, the hydrogen uptake of Pd₉₀Rh₁₀ nanoalloy around 1 bar H₂ pressure is very close to the value of pure Pd. The hydrogen adsorption capacity of pristine carbon is very small, in agreement with our previous report (Zlotea et al., 2015c). The hydrogen uptake increases in the presence of Pd–Rh nanoparticles with the highest enhancement for Pd-rich compositions, despite the increase of the weight of final composites relative to pristine carbon. This might be due to adsorption of molecular H₂ on the developed surfaces of ultrasmall nanoparticles and adsorption in nanoalloys (formation of solid solutions and/or hydride phase). However, the formation

TABLE 1 | Lattice parameter, as obtained from XRD, and average particle size, as determined by TEM.

Sample	Lattice parameter (Å)	Average particle size by TEM (nm)
Bulk Pd	3.891	–
Pd ₉₀ Rh ₁₀	3.89 (1)	1.4 (3)
Pd ₇₅ Rh ₂₅	3.87 (1)	2.0 (6)
Pd ₅₀ Rh ₅₀	3.85 (1)	1.8 (6)
Pd ₂₅ Rh ₇₅	3.83 (1)	2.0 (7)
Pd ₁₀ Rh ₉₀	3.81 (1)	3.0 (1.0)
Bulk Rh	3.80	–

For comparison purposes, the parameters from bulk Pd and Rh are also listed, as taken from Raub (1959) and Noh et al. (1993).

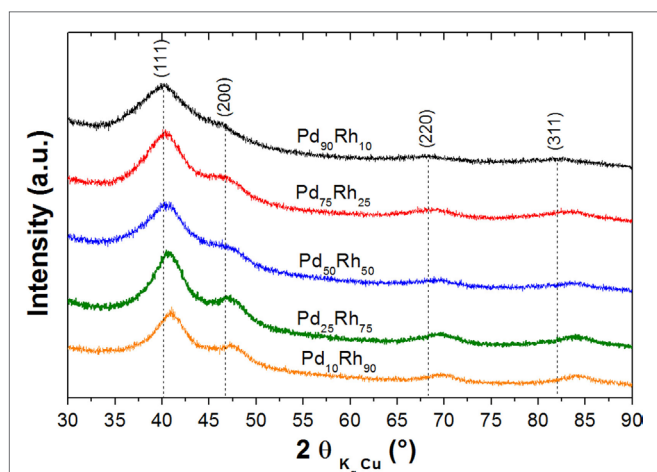


FIGURE 1 | XRD patterns of supported Pd–Rh ultrasmall nanoalloys (reduced at 300°C) with the following compositions: Pd₉₀Rh₁₀, Pd₇₅Rh₂₅, Pd₅₀Rh₅₀, Pd₂₅Rh₇₅, and Pd₁₀Rh₉₀.

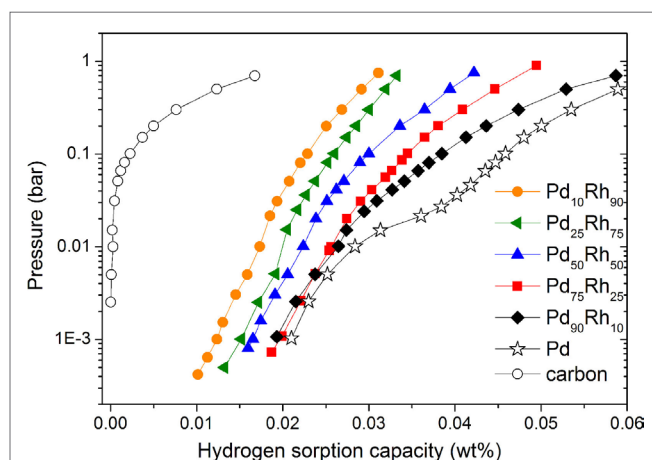


FIGURE 2 | Pressure–composition isotherms at 20°C for all Pd–Rh nanoalloys compared with the pristine carbon (empty circle) and pure Pd nanoparticles with an average size of 2.5 nm (stars).

of hydride phases in these nanoalloys can be excluded due to the absence of equilibrium plateau pressure in the PCI curves, in contrast with pure Pd ultrasmall particles that show a sloped plateau pressure at around 0.02 bar. Despite the presence of an inflection point in the PCI curves of the Pd-rich compositions ($\text{Pd}_{90}\text{Rh}_{10}$, $\text{Pd}_{75}\text{Rh}_{25}$, and $\text{Pd}_{50}\text{Rh}_{50}$), we can conclude that hydrogen uptake in these nanoalloys can be explained by two main mechanisms: hydrogen adsorption (surface reactions) and absorption (formation of solid solutions). Nevertheless, we cannot clearly discriminate between these reactions only from PCI measurements.

To clarify this question, we have performed *in situ* XRD for two Pd-rich nanoalloys ($\text{Pd}_{90}\text{Rh}_{10}$ and $\text{Pd}_{75}\text{Rh}_{25}$) under vacuum and 1 bar H_2 pressure. As noticed in **Figure 3**, XRD diffraction peaks are very broad due to the small nanoparticle sizes, and the most intense peaks (111 and 200) are strongly overlapping, irrespective of the composition and the gaseous environment (vacuum and hydrogen). For the $\text{Pd}_{90}\text{Rh}_{10}$ nanoalloy, a small shift to lower 2θ angles can be noticed for the (111), (220), and (311) peaks confirming hydrogen absorption. Hydrogen atoms are randomly occupying the interstitial sites of the *fcc* structure, and the lattice cell volume is expanding upon absorption. Indeed, the lattice parameter, as refined by the TOPAS software, increases from 3.89 (1) to 3.94 (1) Å under 1 bar H_2 pressure at 20°C. On the contrary, for the $\text{Pd}_{75}\text{Rh}_{25}$ nanoalloy peak displacement is difficult to notice, despite similar PCI curves. Therefore, *in situ* XRD confirms the hydrogen absorption and formation of solid solutions with hydrogen only for the Pd-richest nanoalloy ($\text{Pd}_{90}\text{Rh}_{10}$).

To further discriminate between surface-related reactions and absorption in $\text{Pd}_{75}\text{Rh}_{25}$, $\text{Pd}_{50}\text{Rh}_{50}$, and $\text{Pd}_{25}\text{Rh}_{75}$ nanoalloys, we have carried out in-depth XAS characterization at synchrotron. XAS spectra at the Pd and Rh K edges have been recorded for $\text{Pd}_{75}\text{Rh}_{25}$, $\text{Pd}_{50}\text{Rh}_{50}$, and $\text{Pd}_{25}\text{Rh}_{75}$ nanoalloys under N_2 and H_2 flow at 20°C. The XANES regions show negligible shift, irrespective of the composition and gas atmosphere (Figures S4 and S5 in Supplementary Material).

EXAFS spectra at Pd K edge and corresponding module of the Fourier transform of $\text{Pd}_{75}\text{Rh}_{25}$, $\text{Pd}_{50}\text{Rh}_{50}$, and $\text{Pd}_{25}\text{Rh}_{75}$ nanoalloys

under N_2 and H_2 are shown in **Figure 4**. From EXAFS oscillations at Pd K edge, the Pd atoms environment of the Pd–Rh nanoalloys depends on the gas atmosphere with the strongest effect for $\text{Pd}_{75}\text{Rh}_{25}$. EXAFS spectra at Rh K edge are shown in Figure S6 in Supplementary Material. Contrary to Pd K edge, EXAFS spectra at Rh K edge are very similar, irrespective of composition and gas environment (Figure S6 in Supplementary Material). The results of EXAFS refinements for the first shell of $\text{Pd}_{25}\text{Rh}_{75}$, $\text{Pd}_{50}\text{Rh}_{50}$, and $\text{Pd}_{75}\text{Rh}_{25}$ nanoalloys are listed in **Table 2**.

At Rh K edge, the coordination number N is around 9–10, whereas at Pd K edge N is in between 6 and 8. The decrease of N can be understood by an increased number of dangling bonds due to the large fraction of surface atoms in small clusters (Frenkel et al., 2001; Evans and Tromp, 2008). However, for substitutional alloys, as suggested by XRD, this decrease should affect in the same way N at both Pd and Rh edges. Since N at Pd K edge is smaller than the one at Rh K edge, the local structure of nanoalloys is suggested to be composed of partially segregated Pd-rich surface and Rh-rich core. Similar partial surface segregation of Pd was already proposed for the carbon-supported Pd–Rh alloys with larger nanoparticle size (Oumellal et al. submitted)¹.

At Rh K edge, there are no obvious changes in the Rh–NN distance (2.67–8 Å) and Debye–Waller factor ($\sigma^2 = 0.006\text{--}7 \text{ \AA}^2$), whatever the composition and the atmosphere. At Pd K edge, the Debye–Waller factor under inert gas increases from bulk to nanoparticles (from 0.006 to 0.010 Å², respectively), in agreement with previous studies (Frenkel et al., 2001; Zlotea et al., 2010b). This can be understood in terms of an increase of the static disorder in nanoparticles due to the relaxation of bond lengths at the surface undergoing substantial strain.

The EXAFS results at Pd K edge of Pd–Rh nanoalloys under H_2 atmosphere reveal important modifications. In **Figure 4**, the positions of the main FT peak of $\text{Pd}_{75}\text{Rh}_{25}$ and $\text{Pd}_{50}\text{Rh}_{50}$ nanoalloys under H_2 are slightly shifted to larger distances, as compared

¹Oumellal, Y., Provost, K., Ghimbeu, C. M., Martinez de Yuso, A., and Zlotea, C. (2016). Tailoring hydrogen sorption properties of Pd–Rh nanoalloys (submitted).

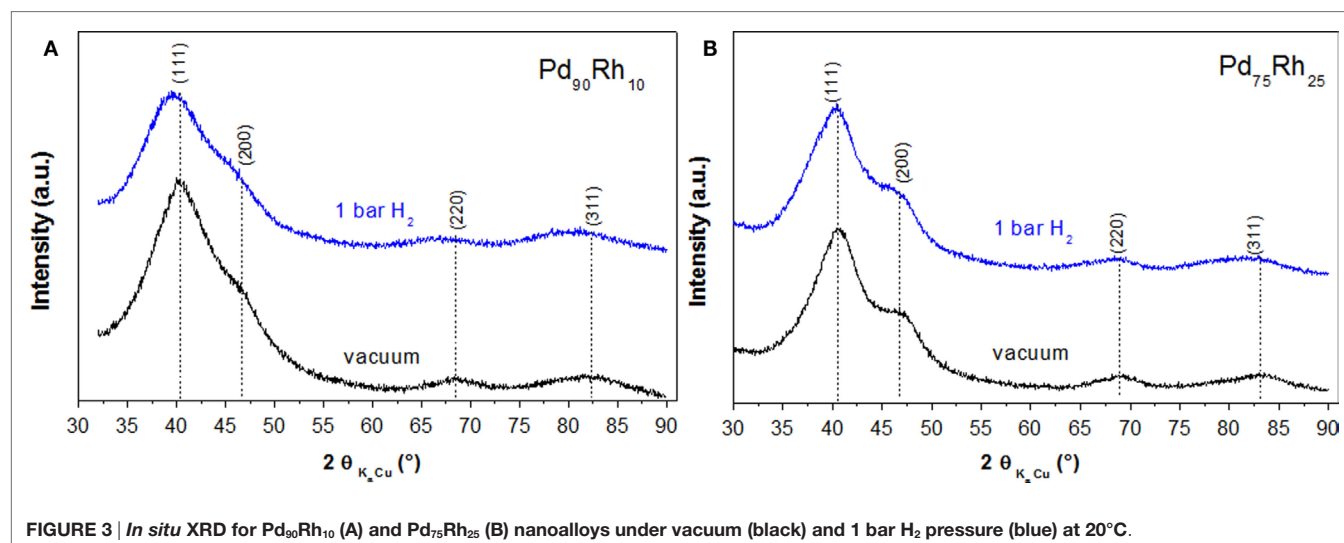


FIGURE 3 | *In situ* XRD for $\text{Pd}_{90}\text{Rh}_{10}$ (A) and $\text{Pd}_{75}\text{Rh}_{25}$ (B) nanoalloys under vacuum (black) and 1 bar H_2 pressure (blue) at 20°C.

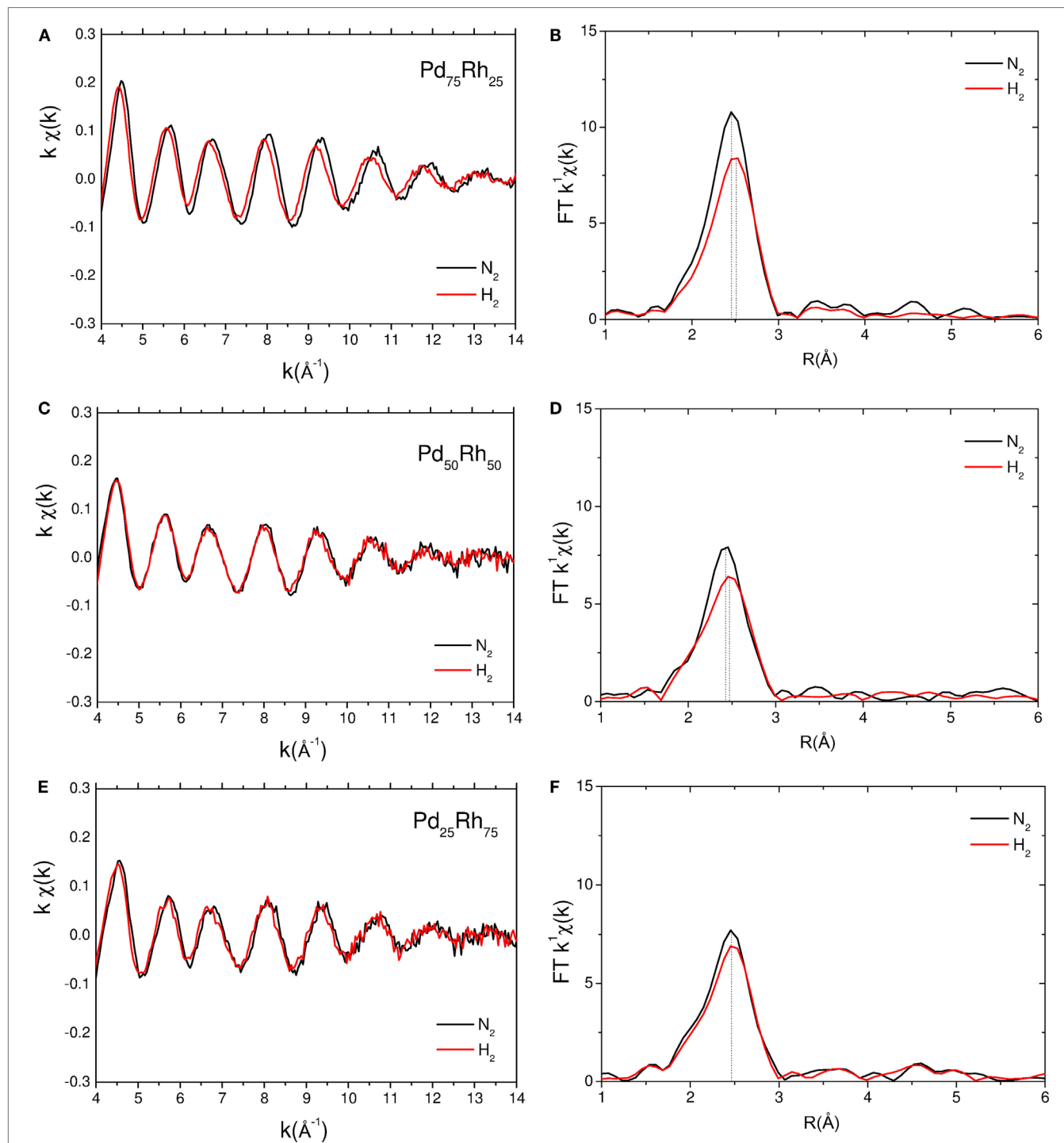


FIGURE 4 | Experimental EXAFS spectra at Pd K edge and corresponding module of the Fourier transform of $\text{Pd}_{75}\text{Rh}_{25}$ (A,B), $\text{Pd}_{50}\text{Rh}_{50}$ (C,D), and $\text{Pd}_{25}\text{Rh}_{75}$ (E,F) under N_2 (black) and H_2 (red) at room temperature. The dotted lines indicate the positions of the main FT peaks.

with the nanoalloys under inert gas. Indeed, an expansion of the $R_{\text{Pd-NN}}$ distances is noticed for $\text{Pd}_{75}\text{Rh}_{25}$ and $\text{Pd}_{50}\text{Rh}_{50}$ under H_2 gas: $\Delta R = 0.03$ and 0.02 \AA , respectively (Table 2). Moreover, since the $R_{\text{Rh-NN}}$ is not affected by the gas environment, this observation suggests that hydrogen atoms preferentially occupy the interstitial

sites in the Pd-rich domains. This finding undoubtedly indicates the occurrence of hydrogen absorption in these ultrasmall nanoparticles and formation of solid solutions with hydrogen. We recall that this conclusion was impossible to state only from PCI and *in situ* XRD measurements. For the Rh-rich nanoalloy

TABLE 2 | Results of EXAFS refinements for the first shell of supported Pd–Rh nanoalloys under different gaseous environments at 20°C: coordination number (N), Debye–Waller factor (σ^2), nearest neighbor distance (R), and the quality of fit (QF).

Sample	Size (nm)	Gas	Pd K edge				Rh K edge			
			N	σ^2 (\AA^2)	$R_{\text{Pd-NN}}$ (\AA)	QF	N	σ^2 (\AA^2)	$R_{\text{Rh-NN}}$ (\AA)	QF
Pd	Bulk	Air	12	0.006 (1)	2.76 (1)	4.5	–	–	–	–
		H ₂ ^a	12 ^a	0.008 (1) ^a	2.84 (1) ^a	–	–	–	–	–
Rh	Bulk	Air	–	–	–	–	12	0.006 (1)	2.69 (1)	3.3
		N ₂	7.6 (1.1)	0.009 (1)	2.75 (1)	0.6	10 (0.9)	0.006 (1)	2.68 (1)	1.6
Pd ₇₅ Rh ₂₅	2.0	H ₂	7.8 (1.6)	0.010 (1)	2.78 (1)	1.0	9 (0.9)	0.007 (1)	2.68 (1)	0.6
		N ₂	6.1 (1.3)	0.010 (1)	2.74 (1)	0.6	8.8 (0.6)	0.006 (1)	2.68 (1)	0.1
Pd ₅₀ Rh ₅₀	1.8	H ₂	7.0 (1.4)	0.011 (1)	2.76 (1)	0.3	8.9 (0.7)	0.006 (1)	2.68 (1)	4.5
		N ₂	6.1 (1.2)	0.009 (1)	2.73 (1)	0.5	9.5 (0.4)	0.006 (1)	2.67 (1)	5.4
Pd ₂₅ Rh ₇₅	2.0	H ₂	6 (1.2)	0.010 (1)	2.74 (1)	0.3	9.4 (0.6)	0.006 (1)	2.68 (1)	5.6

^aResults for bulk Pd under H₂ are also given for comparison from Zlotea et al. (2010b).

studied by EXAFS, the difference between $R_{\text{Pd-NN}}$ distances under N₂ and H₂ gas is within the error bar. Thus, hydrogen adsorption on the developed surface area might account for hydrogen uptake in ultrasmall Rh-rich nanoalloys (Pd₂₅Rh₇₅ and Pd₁₀Rh₉₀), whereas both hydrogen adsorption and absorption (with formation of solid solutions) can explain the hydrogen uptake in Pd-rich nanoalloys (Pd₉₀Rh₁₀, Pd₇₅Rh₂₅, and Pd₅₀Rh₅₀).

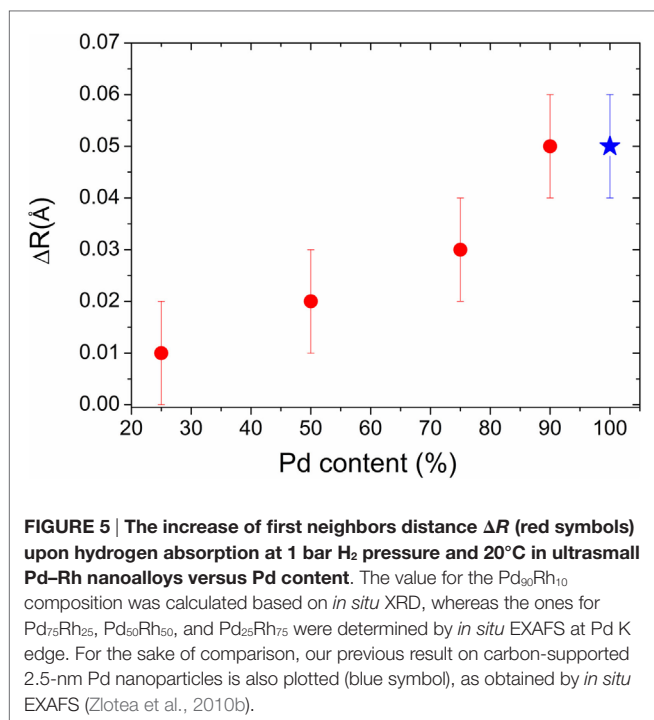
DISCUSSION

The lattice parameters of Pd–Rh nanoparticles, as determined by XRD, vary linearly with the composition (Table 1), as expected for substitutional alloys. The synthetic temperature (300°C) is much lower than the critical temperature of the miscibility gap reported in the bulk Pd–Rh phase diagram (850°C). Thus, these carbon-supported nanoalloys are considered as metastable phases kinetically stabilized in the present synthetic conditions. More discussion about thermodynamic aspects and stability of these phases at nanoscale are detailed in our previous study (Oumellal et al., 2016). As it concerns the local structure of Pd–Rh nanoalloys, EXAFS investigations at both Rh and Pd K edges under inert atmosphere have uncovered a partially segregated structure with Pd-rich surface and Rh-rich core within the nanoparticles.

From PCI investigations (Figure 2), none of Pd–Rh ultrasmall nanoalloys forms a hydride phase under the present conditions (absence of plateau pressure). Interestingly, the composites have higher hydrogen sorption capacities than the pristine carbon despite the increase of weight by insertion of nanoparticles with the most important enhancement for Pd-rich nanoalloys. Both hydrogen adsorption on the surface of nanoalloys and absorption inside the volume of nanoparticles (formation of solid solutions) can account for the enhanced capacities of nanoalloys. However, we cannot discriminate between surface and volume reactions only from PCI measurements. *In situ* XRD under vacuum and 1 bar H₂ pressure provides more information about the hydrogen absorption in the Pd-rich compositions (Figure 3). It is clear that hydrogen absorption and subsequent formation of solid solutions in Pd₉₀Rh₁₀ nanoalloy occur at 1 bar and 20°C. On the contrary, no concluding results could be obtained regarding hydrogen

absorption in the Pd₇₅Rh₂₅ nanoalloy from *in situ* XRD. The final proof of hydrogen absorption and formation of solid solutions in both Pd₇₅Rh₂₅ and Pd₅₀Rh₅₀ nanoalloys was brought by *in situ* EXAFS. Moreover, the latter investigations suggest that hydrogen atoms preferentially occupy the interstitial sites in the Pd-rich domains of these nanoalloys. This is in agreement with the previous report on microsegregation in Pd-rich alloys with Rh induced by hydride formation (Noh et al., 1991).

The chemical composition and the decrease of particle size of Pd–Rh nanoalloys to ultrasmall dimension have drastic consequences on the hydrogen sorption properties. The increase of Rh content in bulk Pd–Rh alloys (maximum 25 at % of Rh) strongly influences the thermodynamic properties of the hydride formation: the enthalpies of hydride formation ($-\Delta H_{\text{hydride}}$) are 37, 30, and 19.4 kJ/molH₂ for pure Pd, Pd₉₀Rh₁₀, and Pd₇₅Rh₂₅ alloys, respectively (Noh et al., 1993). This indicates an increase of the equilibrium pressure of hydride formation from 0.022, 0.480 to 28.3 bar at room temperature (25°C) for pure Pd, Pd₉₀Rh₁₀, and Pd₇₅Rh₂₅ alloys, respectively (Noh et al., 1993; Cappillino et al., 2014). Our recent study on Pd–Rh nanoalloys with large average size (5–6 nm) showed less important thermodynamic changes for the same compositions (See footnote text 1). The values of enthalpy of hydride formation ($-\Delta H_{\text{hydride}}$) are 35 and 30 kJ/molH₂ for Pd₉₀Rh₁₀ (average size 6.4 nm) and Pd₇₅Rh₂₅ (average size 5.5 nm) nanoalloys, respectively. Therefore, the values of the equilibrium plateau pressure of hydride formation correspond to 0.041 and 1.0 bar at room temperature for the Pd₉₀Rh₁₀ and Pd₇₅Rh₂₅ nanoalloys, respectively. Consequently, these nanoalloys with average size around 5–6 nm can form hydride phases under ambient conditions. The destabilization of hydride formation by alloying with Rh is smaller in nanosized Pd–Rh alloys relative to bulk counterparts. In the present case, decreasing the size of Pd–Rh nanoalloys to ultrasmall dimensions (≤ 3 nm) completely suppresses the hydride formation for all compositions. Ultrasmall Pd-rich nanoalloys (Pd₉₀Rh₁₀, Pd₇₅Rh₂₅ and Pd₅₀Rh₅₀) only form solid solutions under ambient conditions, as demonstrated by *in situ* XRD and EXAFS. We hypothesize that the observed hydride suppression in the present Pd-rich nanoparticles might be due to the important stress resulting from their ultrasmall size.



It is obvious that the Pd-Rh nanoalloys chemical composition plays an important role for the hydrogen solubility in the solid solutions formed under ambient conditions. **Figure 5** shows the evolution of ΔR (the increase in first neighbors distance upon hydrogen absorption at 1 bar and 20°C, as calculated based on *in situ* XRD and EXAFS) as function of Pd content in the ultrasmall Pd-Rh nanoalloys. The change in ΔR can be directly related to the hydrogen solubility in solid solutions, which is higher for Pd-rich compositions, in agreement with PCI curves (**Figure 2**). This can be understood in terms of hydrogen preferential occupation in the Pd-rich regions, as suggested by *in situ* EXAFS. Interestingly, the $Pd_{90}Rh_{10}$ nanoalloy can accommodate as much hydrogen-forming solid solutions as pure Pd nanoparticles (2.5 nm) forming a hydride phase under similar conditions, in agreement with the PCI curves in **Figure 2**.

In summary, hydrogen uptake mechanism in ultrasmall Rh-rich nanoalloys ($Pd_{25}Rh_{75}$ and $Pd_{10}Rh_{90}$) is based only on hydrogen adsorption on the developed surface area of nanoparticles, whereas the hydrogen interaction with Pd-rich nanoalloys ($Pd_{90}Rh_{10}$, $Pd_{75}Rh_{25}$, and $Pd_{50}Rh_{50}$) involves both hydrogen adsorption and absorption with formation of solid solutions.

An important aspect of the synthesis and the characterization of such nanomaterials is the coalescence of nanoparticles and formation of large aggregates with bulk-like properties. We have never observed coalescence during repeating measurements/handling of the present Pd-Rh nanoparticles, irrespective of their size and composition. This might be due to the heavy weight of both Pd and Rh atoms that possess very low diffusivity at the present temperatures (20–120°C). This might also explain the formation of metastable phases kinetically stabilized in our synthetic conditions.

CONCLUSION

In the first part of this work, recent advances on synthesis, characterization and hydrogen absorption properties of ultrasmall nanoparticles (defined here as nanoparticles with average size ≤ 3 nm) have been shortly reviewed. The experimental challenges encountered in synthesis, handling, characterization, and accurate determination of hydrogen absorption properties of MgH_2 and noble metal-based ultrasmall nanoparticles have been addressed.

The second part reports original results obtained for carbon-supported ultrasmall Pd-Rh nanoalloys. We have successfully prepared ultrasmall Pd-Rh nanoalloys by liquid impregnation method followed by reduction at 300°C, despite the large miscibility gap in the bulk Pd-Rh phase diagram (with the critical temperature $\sim 850^\circ C$). EXAFS investigations suggest that the local structure of these nanoalloys is partially segregated into Rh-rich core and Pd-rich surface.

Downsizing to ultrasmall dimensions induces drastic modifications of hydrogen absorption properties of Pd-Rh alloys and completely suppresses the hydride formation for all compositions of ultrasmall nanoparticles, as observed by the PCI measurements at ambient conditions. This finding is in contrast with both bulk alloys and larger sized nanoalloys (5–6 nm): Pd-rich compositions ($Pd_{90}Rh_{10}$ ~ 6.4 nm and $Pd_{75}Rh_{25}$ ~ 5.5 nm) form hydride phases under similar conditions. Ultrasmall $Pd_{90}Rh_{10}$, $Pd_{75}Rh_{25}$, and $Pd_{50}Rh_{50}$ nanoalloys absorb hydrogen-forming solid solutions at atmospheric pressure and room temperature. The hydrogen solubility in solid solutions is higher for Pd-rich compositions. This can be understood in terms of hydrogen preferential occupation in the Pd-rich regions, as suggested by *in situ* EXAFS. The Rh-rich nanoalloys only adsorb hydrogen on the developed surfaces of ultrasmall nanoparticles.

These results have been highlighted by combined laboratory and large-scale facility technique, such as *in situ* EXAFS. Apart from the Pd-richest composition, common laboratory techniques, such as *in situ* XRD, DSC, and PCI, could not distinguish between hydrogen adsorption on surface and hydrogen absorption in volume accompanied by formation of solid solutions. Therefore, it is obvious that the rising need for *in situ* characterization methods provided by large-scale facilities to explore the hydrogen interaction with ultrasmall nanoparticles. This is an important topic of fundamental research not only for solid-state hydrogen storage materials and sensors but also for heterogeneous catalysis, given that ultrasmall Pd-based nanoparticles are widely used for many chemical reactions involving hydrogen.

AUTHOR CONTRIBUTIONS

CZ ensured the direction of the research project, performed the XAS experiments and EXAFS refinements, and provided necessary opportunities for fruitful discussion among authors. YO performed the synthesis and characterization of all composite materials and participated to XAS experiments. KP helped for XAS experiments, analysis, and EXAFS refinements. CG carried out the synthesis and the characterization of pristine porous carbon support as well as the EDX chemical mapping for composite materials.

ACKNOWLEDGMENTS

Fabrice Couturas is warmly acknowledged for help during *in situ* XAS experiments at Soleil. The authors thank Julie Bourgon (ICMPE) and Loïc Vidal (IS2M) for TEM measurements.

FUNDING

The work was funded by the French National Research Agency (ANR) under GENESIS project contract no 13-BS08-0004.

REFERENCES

- Ankudinov, A. L., Nesvizhskii, A. I., and Rehr, J. J. (2003). Dynamic screening effects in x-ray absorption spectra. *Phys. Rev. B* 67, 115120. doi:10.1103/PhysRevB.67.115120
- Ankudinov, A. L., Ravel, B., Rehr, J. J., and Conradson, S. D. (1998). Real-space multiple-scattering calculation and interpretation of x-ray-absorption near-edge structure. *Phys. Rev. B* 58, 7565–7576. doi:10.1103/PhysRevB.58.7565
- Au, Y. S., Obbink, M. K., Srinivasan, S., Magusin, P. C. M. M., de Jong, K. P., and de Jongh, P. E. (2014). The size dependence of hydrogen mobility and sorption kinetics for carbon-supported MgH₂ particles. *Adv. Funct. Mater.* 24, 3604–3611. doi:10.1002/adfm.201304060
- Bastide, S., Zlotea, C., Laurent, M., Latroche, M., and Cachet-Vivier, C. (2013). Direct assessment from cyclic voltammetry of size effect on the hydrogen sorption properties of Pd nanoparticle/carbon hybrids. *J. Electroanal. Chem.* 706, 33–39. doi:10.1016/j.jelechem.2013.07.036
- Bérubé, V., Radtke, G., Dresselhaus, M., and Chen, G. (2007). Size effects on the hydrogen storage properties of nanostructured metal hydrides: a review. *Int. J. Energy Res* 31, 637–663. doi:10.1002/er.1284
- Borgschulte, A. (2016). The hydrogen grand challenge. *Front. Energy Res.* 4:11. doi:10.3389/fenrg.2016.00011
- Campesi, R., Cuevas, F., Gadiou, R., Leroy, E., Hirscher, M., Vix-Guterl, C., et al. (2008). Hydrogen storage properties of Pd nanoparticle/carbon template composites. *Carbon N. Y.* 46, 206–214. doi:10.1016/j.carbon.2007.11.006
- Cappillino, P. J., Lavernia, E. J., Ong, M. D., Wolfer, W. G., and Yang, N. Y. (2014). Plastic deformation and hysteresis for hydrogen storage in Pd-Rh alloys. *J. Alloys Compd.* 586, 59–65. doi:10.1016/j.jallcom.2013.10.033
- Cheng, F., Tao, Z., Liang, J., and Chen, J. (2012). Efficient hydrogen storage with the combination of lightweight Mg/MgH₂ and nanostructures. *Chem. Commun.* 48, 7334–7343. doi:10.1039/c2cc30740e
- Contescu, C. I., van Benthem, K., Li, S., Bonifacio, C. S., Pennycook, S. J., Jena, P., et al. (2011). Single Pd atoms in activated carbon fibers and their contribution to hydrogen storage. *Carbon N. Y.* 49, 4050–4058. doi:10.1016/j.carbon.2011.05.021
- Crivello, J.-C., Dam, B., Denys, R. V., Dornheim, M., Grant, D. M., Huot, J., et al. (2016). Review of magnesium hydride-based materials: development and optimisation. *Appl. Phys. A* 122, 97. doi:10.1007/s00339-016-9602-0
- de Jongh, P. E., and Adelhelm, P. (2010). Nanosizing and nanoconfinement: new strategies towards meeting hydrogen storage goals. *ChemSusChem* 3, 1332–1348. doi:10.1002/cssc.201000248
- de Jongh, P. E., Allendorf, M., Vajo, J. J., and Zlotea, C. (2013). Nanoconfined light metal hydrides for reversible hydrogen storage. *MRS Bull.* 38, 488–494. doi:10.1557/mrs.2013.108
- de Jongh, P. E., and Eggenhuisen, T. M. (2013). Melt infiltration: an emerging technique for the preparation of novel functional nanostructured materials. *Adv. Mater.* 25, 6672–6690. doi:10.1002/adma.201301912
- de Jongh, P. E., Wagemans, R. W. P., Eggenhuisen, T. M., Dauvillier, B. S., Radstake, P. B., Meeldijk, J. D., et al. (2007). The preparation of carbon-supported magnesium nanoparticles using melt infiltration. *Chem. Mater.* 19, 6052–6057. doi:10.1021/cm702205v
- Driessen, A., Sanger, P., Hemmes, H., and Griessen, R. (1990). Metal hydride formation at pressures up to 1Mbar. *J. Phys. Condens. Matter* 2, 9797–9814. doi:10.1088/0953-8984/2/49/007

As it concerns the access and use of ROCK beam line at SOLIL synchrotron, this work was supported by a public grant overseen by the French National Research Agency (ANR) as part of the “Investissements d’Avenir” program (reference: ANR-10-EQPX-45).

SUPPLEMENTARY MATERIAL

The Supplementary Material for this article can be found online at <http://journal.frontiersin.org/article/10.3389/fenrg.2016.00024>

- Eberle, U., Felderhoff, M., and Schuth, F. (2009). Chemical and physical solutions for hydrogen storage. *Angew. Chem. Int. Ed.* 48, 6608–6630. doi:10.1002/anie.200806293
- Essinger-Hileman, E. R., DeCicco, D., Bondi, J. F., and Schaak, R. E. (2011). Aqueous room-temperature synthesis of Au-Rh, Au-Pt, Pt-Rh, and Pd-Rh alloy nanoparticles: fully tunable compositions within the miscibility gaps. *J. Mater. Chem.* 21, 11599–11604. doi:10.1039/c0jm03913f
- Evans, J., and Tromp, M. (2008). Interaction of small gas phase molecules with alumina supported rhodium nanoparticles: an *in situ* spectroscopic study. *J. Phys. Condens. Matter* 20, 184020. doi:10.1088/0953-8984/20/18/184020
- Fontaine, C. L., Barthe, L., Rochet, A., and Briois, V. (2013). X-ray absorption spectroscopy and heterogeneous catalysis: performances at the SOLEIL’s SAMBA beamline. *Catal. Today* 205, 148–158. doi:10.1016/j.cattod.2012.09.032
- Frenkel, A. I., Hills, C. W., and Nuzzo, R. G. (2001). A view from the inside: complexity in the atomic scale ordering of supported metal nanoparticles. *J. Phys. Chem. B* 105, 12689–12703. doi:10.1021/jp012769j
- Ghimbeu, C. M., Zlotea, C., Gadiou, R., Cuevas, F., Leroy, E., Latroche, M., et al. (2011). Understanding the mechanism of hydrogen uptake at low pressure in carbon/palladium nanostructured composites. *J. Mater. Chem.* 21, 17765–17775. doi:10.1039/c1jm12939b
- Kobayashi, H., Yamauchi, M., and Kitagawa, H. (2012a). Finding hydrogen-storage capability in iridium induced by the nanosize effect. *J. Am. Chem. Soc.* 134, 6893–6895. doi:10.1021/ja302021d
- Kobayashi, H., Morita, H., Yamauchi, M., Ikeda, R., Kitagawa, H., Kubota, Y., et al. (2012b). Nanosize-induced drastic drop in equilibrium hydrogen pressure for hydride formation and structural stabilization in Pd-Rh solid-solution alloys. *J. Am. Chem. Soc.* 134, 12390–12393. doi:10.1021/ja305031y
- Konarova, M., Tanksale, A., Norberto Beltramini, J., and Qing Lu, G. (2012). Effects of nano-confinement on the hydrogen desorption properties of MgH₂. *Nano Energy* 2, 98–104. doi:10.1016/j.nanoen.2012.07.024
- Langhammer, C., Zhdanov, V. P., Zoric, I., and Kasemo, B. (2010). Size-dependent kinetics of hydriding and dehydriding of Pd nanoparticles. *Phys. Rev. Lett.* 104, 135502. doi:10.1103/PhysRevLett.104.135502
- Michalowicz, A., Moscovici, J., Muller-Bouvet, D., and Provost, K. (2009). MAX: multiplatform applications for XAFS. *J. Phys. Conf. Ser.* 190, 012034. doi:10.1088/1742-6596/190/1/012034
- Michalowicz, A., Moscovici, J., Muller-Bouvet, D., and Provost, K. (2013). MAX (multiplatform applications for XAFS) new features. *J. Phys. Conf. Ser.* 430, 012016. doi:10.1088/1742-6596/430/1/012016
- Moretto, P., Zlotea, C., Dolci, F., Amieiro, A., Bobet, J.-L., Borgschulte, A., et al. (2013). A round Robin test exercise on hydrogen absorption/desorption properties of a magnesium hydride based material. *Int. J. Hydrogen Energy* 38, 6704–6717. doi:10.1016/j.ijhydene.2013.03.118
- Narehood, D. G., Kishore, S., Goto, H., Adair, J. H., Nelson, J. A., Gutierrez, H. R., et al. (2009). X-ray diffraction and H-storage in ultra-small palladium particles. *Int. J. Hydrogen Energy* 34, 952–960. doi:10.1016/j.ijhydene.2008.10.080
- Nielsen, T. K., Manickam, K., Hirscher, M., Besenbacher, F., and Jensen, T. R. (2009). Confinement of MgH₂ nanoclusters within nanoporous aerogel scaffold materials. *ACS Nano* 3, 3521–3528. doi:10.1021/nm901072w
- Noh, H., Flanagan, T. B., Cerundolo, B., and Craft, A. (1991). Hydrogen-induced metal atom mobility in palladium-rhodium alloys. *Scr. Metall. Mater.* 25, 225–230. doi:10.1016/0956-716X(91)90385-E

- Noh, H., Luo, W., and Flanagan, T. B. (1993). The effect of annealing pretreatment of Pd-Rh alloys on their hydrogen solubilities and thermodynamic parameters for H₂ solution. *J. Alloys Compd.* 196, 7–16. doi:10.1016/0925-8388(93)90562-2
- Oumellal, Y., Joubert, J.-M., Matei Ghimbeu, C., Le Meins, J.-M., Bourgon, J., and Zlotea, C. (2016). Synthesis and stability of Pd-Rh nanoalloys with fully tunable particle size and composition. *Nano-Structures & Nano-Objects*. doi:10.1016/j.nanos.2016.06.005
- Oumellal, Y., Zlotea, C., Bastide, S., Cachet-Vivier, C., Leonel, E., Sengmany, S., et al. (2014). Bottom-up preparation of MgH₂ nanoparticles with enhanced cycle life stability during electrochemical conversion in Li-ion batteries. *Nanoscale* 6, 14459–14466. doi:10.1039/C4NR03444A
- Pundt, A., and Kirchheim, R. (2006). Hydrogen in metals: microstructural aspects. *Annu. Rev. Mater. Res.* 36, 555–608. doi:10.1146/annurev.matsci.36.090804.094451
- Raub, E. (1959). Metals and alloys of the platinum group. *J. Less Common Met.* 1, 3–18. doi:10.1016/0022-5088(59)90014-1
- Roduner, E. (2006). Size matters: why nanomaterials are different. *Chem. Soc. Rev.* 35, 583–592. doi:10.1039/b502142c
- Roesler, C., and Fischer, R. A. (2015). Metal-organic frameworks as hosts for nanoparticles. *CrystEngComm* 17, 199–217. doi:10.1039/C4CE01251H
- Sachs, C., Pundt, A., Kirchheim, R., Winter, M., Reetz, M. T., and Fritsch, D. (2001). Solubility of hydrogen in single-sized palladium clusters. *Phys. Rev. B* 64, 075408. doi:10.1103/PhysRevB.64.075408
- Sartori, S., Cuevas, F., and Latroche, M. (2016). Metal hydrides used as negative electrode materials for Li-ion batteries. *Appl. Phys. A* 122, 1–7. doi:10.1007/s00339-016-9674-x
- Sayers, D. E. (2000). *Report of the International XAFS Society Standards and Criteria Committee*. Available at: http://ixs.iit.edu/subcommittee_reports/sc/SC00report.pdf
- Wilcoxon, J. P., and Abrams, B. L. (2006). Synthesis, structure and properties of metal nanoclusters. *Chem. Soc. Rev.* 35, 1162–1194. doi:10.1039/b517312b
- Yamauchi, M., Ikeda, R., Kitagawa, H., and Masaki, T. (2008). Nanosize effects on hydrogen storage in palladium. *J. Phys. Chem. C* 112, 3294–3299. doi:10.1021/jp710447j
- Zhang, S., Gross, A. F., Van Atta, S. L., Lopez, M., Liu, P., Ahn, C. C., et al. (2009). The synthesis and hydrogen storage properties of a MgH₂ incorporated carbon aerogel scaffold. *Nanotechnology* 20, 204027. doi:10.1088/0957-4484/20/20/204027
- Zhao, W., Fierro, V., Zlotea, C., Izquierdo, M. T., Chevalier-Cesar, C., Latroche, M., et al. (2012). Activated carbons doped with Pd nanoparticles for hydrogen storage. *Int. J. Hydrogen Energy* 37, 5072–5080. doi:10.1016/j.ijhydene.2011.12.058
- Zlotea, C., Campesi, R., Cuevas, F., Leroy, E., Dibandjo, P., Volkringer, C., et al. (2010a). Pd nanoparticles embedded into a metal-organic framework: synthesis, structural characteristics, and hydrogen sorption properties. *J. Am. Chem. Soc.* 132, 2991–2997. doi:10.1021/ja9084995
- Zlotea, C., Cuevas, F., Paul-Boncour, V., Leroy, E., Dibandjo, P., Gadiou, R., et al. (2010b). Size-dependent hydrogen sorption in ultrasmall Pd clusters embedded in a mesoporous carbon template. *J. Am. Chem. Soc.* 132, 7720–7729. doi:10.1021/ja101795g
- Zlotea, C., Chevalier-Cesar, C., Leonel, E., Leroy, E., Cuevas, F., Dibandjo, P., et al. (2011). Synthesis of small metallic Mg-based nanoparticles confined in porous carbon materials for hydrogen sorption. *Faraday Discuss.* 151, 117–131. doi:10.1039/c0fd00016g
- Zlotea, C., Cuevas, F., Andrieux, J., Ghimbeu, C. M., Leroy, E., Leonel, E., et al. (2013). Tunable synthesis of (Mg-Ni)-based hydrides nanoconfined in templated carbon studied by in situ synchrotron diffraction. *Nano Energy* 2, 12–20. doi:10.1016/j.nanoen.2012.07.005
- Zlotea, C., and Latroche, M. (2013). Role of nanoconfinement on hydrogen sorption properties of metal nanoparticles hybrids. *Colloids Surf. A Physicochem. Eng. Asp.* 439, 117–130. doi:10.1016/j.colsurfa.2012.11.043
- Zlotea, C., Morfin, F., Nguyen, T. S., Nguyen, N. T., Nelayah, J., Ricolleau, C., et al. (2014). Nanoalloying bulk-immiscible iridium and palladium inhibits hydride formation and promotes catalytic performances. *Nanoscale* 6, 9955–9959. doi:10.1039/c4nr02836h
- Zlotea, C., Oumellal, Y., Hwang, S.-J., Ghimbeu, C. M., de Jongh, P. E., and Latroche, M. (2015a). Ultrasmall MgH₂ nanoparticles embedded in an ordered microporous carbon exhibiting rapid hydrogen sorption kinetics. *J. Phys. Chem. C* 119, 18091–18098. doi:10.1021/acs.jpcc.5b05754
- Zlotea, C., Oumellal, Y., Msakni, M., Bourgon, J., Bastide, S., Cachet-Vivier, C., et al. (2015b). First evidence of Rh nano-hydride formation at low pressure. *Nano Lett.* 15, 4752–4757. doi:10.1021/acs.nanolett.5b01766
- Zlotea, C., Ghimbeu, C. M., Oumellal, Y., Crivello, J.-C., Vix-Guterl, C., and Latroche, M. (2015c). Hydrogen sorption properties of Pd-Co nanoalloys embedded into mesoporous carbons. *Nanoscale* 7, 15469–15476. doi:10.1039/c5nr03143e

Conflict of Interest Statement: The authors declare that the research was conducted in the absence of any commercial or financial relationships that could be construed as a potential conflict of interest.

Copyright © 2016 Zlotea, Oumellal, Provost and Ghimbeu. This is an open-access article distributed under the terms of the Creative Commons Attribution License (CC BY). The use, distribution or reproduction in other forums is permitted, provided the original author(s) or licensor are credited and that the original publication in this journal is cited, in accordance with accepted academic practice. No use, distribution or reproduction is permitted which does not comply with these terms.